

ALTERATIONS IN OSTEOCYTE LACUNAR MORPHOLOGY AFFECT LOCAL BONE TISSUE STRAINS

Haniyeh Hemmatian^{1,2,3}, Astrid D Bakker², Jenneke Klein-Nulend², G. Harry van Lenthe¹

¹ Biomechanics Section, Department of Mechanical Engineering, KU Leuven, Leuven, Belgium

² Department of Oral Cell Biology, Academic Centre for Dentistry Amsterdam (ACTA), University of Amsterdam and Vrije Universiteit Amsterdam, Amsterdam Movement Sciences, Amsterdam, The Netherlands

³ Department of Osteology and Biomechanics, University Medical Center Hamburg-Eppendorf, Hamburg, Germany.

Corresponding author:

G. Harry van Lenthe, PhD

Biomechanics section

Department of Mechanical Engineering

KU Leuven

Celestijnenlaan 300

3001 Leuven

Belgium

Tel +32 16 32 25 95

Fax +32 16 32 79 94 Email:

harry.vanlenthe@kuleuven.be

ABSTRACT

Osteocytes are capable of remodeling their perilacunar bone matrix, which causes considerable variations in the shape and size of their lacunae. If these variations in lacunar morphology cause changes in the mechanical environment of the osteocytes, in particular local strains, they would subsequently affect bone mechanotransduction, since osteocytes are likely able to directly sense these strains. The purpose of this study is to quantify the effect of alterations in osteocyte lacunar morphology on perilacunar bone tissue strains. To this end, we related the actual lacunar shape in fibulae of six young-adult (5-month) and six old (23-month) mice, quantified by high-resolution micro-computed tomography, to microscopic strains, analyzed by micro-finite element modeling. We showed that peak effective strain increased by 12.6% in osteocyte cell bodies (OCYs), 9.6% in pericellular matrix (PCM), and 5.3% in extra cellular matrix (ECM) as the lacunae volume increased from 100-200 μm^3 to 500-600 μm^3 . Lacunae with a larger deviation ($> 8^\circ$) in orientation from the longitudinal axis of the bone are exposed to 8% higher strains in OCYs, 6.5% in PCM, 4.2% in ECM than lacunae with a deviation in orientation below 8 degrees. Moreover, increased lacuna sphericity from 0-0.5 to 0.7-1 led to 25%, 23%, and 13% decrease in maximum effective strains in OCYs, PCM, and ECM, respectively. We further showed that due to the presence of smaller and more round lacunae in old mice, local bone tissue strains are on average 5% lower in the vicinity of lacunae and their osteocytes of old mice compared to young. Understanding how changes in lacunar morphology affect the micromechanical environment of osteocytes presents a first step in unraveling their potential role in impaired bone mechanoresponsiveness with e.g. aging.

KEY WORDS

Osteocyte lacunar morphology, local bone tissue strain, micro-finite element analysis, high resolution micro-computed tomography

HIGHLIGHTS

1. Variations in the morphology of lacunae resulted in alterations in local strain amplification.
2. Lacunae with a larger volume, more closely aligned with the longitudinal axis of the bone, and more elongated are exposed to higher strains.
3. Age-related changes in lacunar shape result in slightly lower local bone tissue strains.

1. INTRODUCTION

Bone is a dynamic tissue, able to adapt its mechanical environment throughout daily life. Bone adaptation is achieved by the bone remodeling process, which is regulated by the highly mechanosensitive osteocytes, residing throughout the bone matrix. Osteocytes reside in cavities within the bone matrix called lacunae, and are connected to each other through small canals named canaliculi, thus forming the lacuno-canalicular network. Through this extensive communication network, the osteocytes sense mechanical signals and coordinate the recruitment and activity of bone resorbing osteoclasts and/or bone forming osteoblasts through the production of a multitude of signaling molecules (Klein-Nulend et al., 2013, 2012). Osteocytes thus orchestrate the adaptation of bone mass and structure in response to mechanical signals.

Osteocytes can sense fluid flow-induced shear stress, bone-loading induced hydrostatic pressure, as well as loading-induced matrix strains (Burger and Klein-Nulend, 1999; Klein-Nulend et al., 2013, 2012). Although bulk matrix strains may be too low to be sensed by osteocyte cells residing in the matrix, the lacuna-canalicular network amplify the strains to magnitudes that are likely to be biologically relevant. Interestingly, the morphology of lacunae could influence the strain amplification around the cell body and the transmission of strain to the immediate osteocyte microenvironment, thus affecting the magnitude of the stimulus (Bonivitch et al., 2007; Nicolella et al., 2006; Verbruggen et al., 2015). Osteocytes are likely capable of sensing local bone matrix strains directly through their cell body via integrins and focal adhesion complexes which mechanically link the cytoskeleton in the osteocyte extensions and cell body to the extracellular matrix (Bacabac et al., 2008; Chen et al., 2004; Klein-Nulend et al., 2012; Aviral Vatsa et al., 2008; Wang et al., 1993). Thus,

osteocytes of different shapes and sizes, with different shapes and sizes of the lacuna-canalicular network could experience a locally modified mechanical environment, and would react with a modified mechanoreponse, with consequences for bone mass, architecture, and thus fracture resistance, but to what extent remains to be determined.

A direct quantification of the micromechanical environment of the osteocytes embedded in a mineralized bone matrix is challenging, if not impossible. As an alternative, efforts have been made to measure the three-dimensional local bone tissue strains and stresses around osteocytes and their adaptive response to imposed macroscopic deformations using computational models (Bonivtch et al., 2007; Varga et al., 2015; Vaughan et al., 2013; Wang et al., 2015). Thus far, these studies have mainly evaluated idealized lacuno-canalicular network geometries, affecting the reliability and accuracy of finite element (FE) analysis; indeed, large variations have been found between results achieved from idealized and more realistic models (Anderson and Knothe Tate, 2008; Schneider et al., 2012; Varga et al., 2015; Verbruggen et al., 2012; Wang et al., 2015). Yet, the studies using highly-detailed and accurate computational models have been limited in their analysis of a few single lacunae only. Thus, since lacunae show a broad spectrum in sizes and in shapes, and since their deformation is affected by neighbouring microporosity (Vaughan et al., 2013), computational models closely mimicking the actual lacuna and vascular canal network geometry are highly desirable. To this end, in this study, we aimed to take advantage of voxel-based FE modelling of the entire mouse cortical bone microstructures including realistic geometries of lacunae and vascular canal networks to quantify the effect of alterations in osteocyte lacunar network morphology and heterogeneity on peri-lacunar bone tissue strains. The advantage of modeling the

entire cortical bone microporosities was that the effect of microporosities including osteocyte lacunae and vascular canals as potential stress concentrators on the predicted local tissue strain were taken into account.

2. MATERIALS AND METHODS

2.1. Specimens

Mice used in the current study had been used in a previous study (Hemmatian et al., 2018b) ethically approved by the Animal Ethics Committee of KU Leuven (P075/2015). Briefly, one fibula per animal was extracted from twelve female C57BL/6JRccHsd mice. Six animals were 5-months of age ('Young'); six others were 23-months of age ('Old').

2.2. Micro-computed tomography imaging

In a recently published study (Hemmatian et al., 2018b), we used micro-computed tomography (μ CT) imaging to investigate age-related changes in female mouse cortical bone microporosity. Briefly, the mid-section of each fibula was scanned using a SkyScan 1172 (Bruker, Kontich, Belgium) μ CT scanner. The scan area started at 50% of the whole fibula length (calculated from the growth plate at the proximal part) minus 0.7 mm. 2000 contiguous slices with a nominal isotropic resolution of 0.7 μ m were made, resulting in a stack height of 1.4 mm.

Segmentation of cortical bone (extra cellular matrix (ECM)) was performed using our previously reported technique (Hemmatian et al., 2017). Intracortical porosity comprising lacunae and vascular canals were identified by inverting the image and using the 3D despeckle filter in CTAn software (SkyScan). The objects less than 100 μm^3 were considered to be noise, elements with a volume in the range between 100 and 2000 μm^3 were assumed to be lacunae, and the objects greater than 2000 μm^3 were considered to be vascular canals. These volume limits were based on the confocal microscopy measurements indicating a size between 28-1713 μm^3 for each

osteocyte (McCreadie et al., 2004). We derived morphometric measures for the ECM and lacunar network using CTAn, including cortical bone volume fraction (Ct.BV/TV), cortical bone microporosity (including vascular canal porosity and lacuna porosity), lacuna number density (N.Lc/Ct.TV), individual lacuna volume (Lc.V), lacuna orientation (Lc.θ), and lacuna sphericity (Lc.Sph). The lacuna orientation was calculated with respect to the longitudinal axis of the fibula and determined by the main eigenvalues of the second moments of inertia of each lacuna. The lacuna sphericity was calculated as the ratio of the surface area of a sphere with the same volume as the given lacuna to the lacuna surface area. Furthermore, using a combination of morphological operations in MATLAB (an erosion operation followed by Boolean subtraction operation), the pericellular matrix (PCM) and osteocyte cell bodies (OCYs) were segmented to be included in the FE modeling. The PCM was identified as the volume obtained after operation of 1 voxel (0.7 μm) erosion of the lacuna space (McNamara et al., 2009; Vaughan et al., 2013; Verbruggen et al., 2012); the remaining volume of the lacuna space was considered as OCY.

2.3. Microstructural finite element analysis

μFE models of the bone ECM, PCM and OCYs were created by a direct conversion of μCT-image isotropic voxels with a size of 0.7 μm to 8-node linear hexahedral elements (van Rietbergen et al., 1995). The μFE models contained the central 500 μCT image slices of each fibula (representing a stack of 0.35 mm; Fig. 1 A). To create FE meshes a custom-built in-house mesher was used. On average, the μFE models consisted of 105 million and 132 million elements for young and old mice, respectively. The ECM, PCM and OCYs material properties were assumed to be homogeneous, linear, and isotropic with a Young's moduli of 16 GPa, 40 kPa, and 4.47 kPa, respectively and

Poisson ratio of 0.3 for all materials (Varga et al., 2015; Verbruggen et al., 2012). The top surface of the models was loaded by a prescribed uniaxial displacement resulting in 1% apparent compressive strain along the fibula longitudinal direction (Fig. 1 A). All nodes on the bottom surface were constrained against the direction of applied displacement except for two nodes which were fixed in the transversal plane too, in order to prevent rigid body rotation and translations. Models were solved in less than 10 min with the fully parallel linear finite element solver ParOsol (Flaig and Arbenz, 2011) using 90 CPUs (Cray XC40/XC50) at the Swiss National Supercomputing Centre (CSCS, Lugano, Switzerland). The micromechanical environment of each lacuna was characterized in terms of effective strains (EFF) (Pistoia et al., 2002) and strain amplification. Effective strain was calculated from the strain-energy density (U) and the Young's modulus (E) of the bone tissue as follows: $EFF = \sqrt{2U/E}$. The effective strain has been selected as the mechanical parameter to analyze local bone tissue strains around lacunae since it is a scalar value based on deformation energy summarizing the strain tensor due to different loading conditions through either bone matrix deformation or interstitial fluid flow. The strain amplification factor was calculated as the local effective strain divided by the applied global strain (Bonivitch et al., 2007). The strain amplification was quantified as a function of distance from the lacuna boundary. As the maximum and minimum EFF strain distribution were strongly dependent on the distance from the lacuna boundary, and the peak strains were observed in the direct vicinity of the lacunae, the maximum and minimum EFF strain amplifications were quantified within the 0.7 μm vicinity of each lacuna boundary as a function of Lc.V, Lc.Sph and Lc. Θ . **The maximum and minimum effective strains per individual lacuna were averaged over top and bottom 0.1% of EFF strains identified in different regions, respectively.** Furthermore, the percentage of osteocyte volume

exposed to a specific effective strain was calculated as the portion of voxels representing osteocytes experiencing a specific effective strain magnification. All these post-processing analyses were performed using Matlab (The Mathworks Inc., Natick, MA, USA). In addition to analyses of the local bone tissue strain in the midshaft of the fibula, a regional sub analysis in the anterior and posterior sites exposed to compression and tension (Torcasio et al., 2012) was performed. The anterior and posterior sites were defined by the lateral-medial axis passing through the centroid. Moreover, to evaluate the effect of finite element size on the results, a mesh refinement study has been performed. A sub-volume of 250 μ CT image slices of each fibula was remeshed by subdividing every image voxels into 8 mesh voxels, resulting in models containing up to 532 million elements. The EFF strains calculated in the submodels were compared to those in the corresponding part of the coarser original models.

2.4. Statistics

Statistical analyses were performed using GraphPad Prism version 6.0 for Windows (GraphPad Software, La Jolla, CA, USA). To assess the significant differences in maximum and minimum EFF strains in between ECM, PCM and OCY as well as to evaluate the effect of aging, a two-way analysis of variance followed by Tukey multiple comparisons test was used. A multiple regression analysis was performed to determine which lacunar morphological parameters were correlated to local bone tissue strains. The effect of lacunar morphology on the maximum EFF strains were assessed using one-way repeated-measures ANOVA, followed by Tukey's multiple comparisons test. The same test was used to assess the effect of increasing distance from lacunar surface on the maximum and minimum EFF strains. Differences in maximum effective strain due to age and anatomic sites were assessed using a two-

way analysis of variance, followed by Tukey multiple comparisons test. All tests were considered significant at $p < 0.05$. Data are averaged over the entire lacunae in each bone and presented as mean \pm SD.

3. RESULTS

EFF strains in ECM, PCM and OCYs were successfully calculated for all bone samples. Qualitatively, it can be seen from Fig. 1 C,D that the high EFF strains in ECM are concentrated around intracortical porosities including lacunae and vascular canals. Minimum effective strains were seen at the tips of the lacunae, whereas maximum effective strains were found perpendicular to the long axis of lacunae. The presence of lacunae and vascular canals under each surface affect the EFF strain distribution (Fig. 1 C,D).

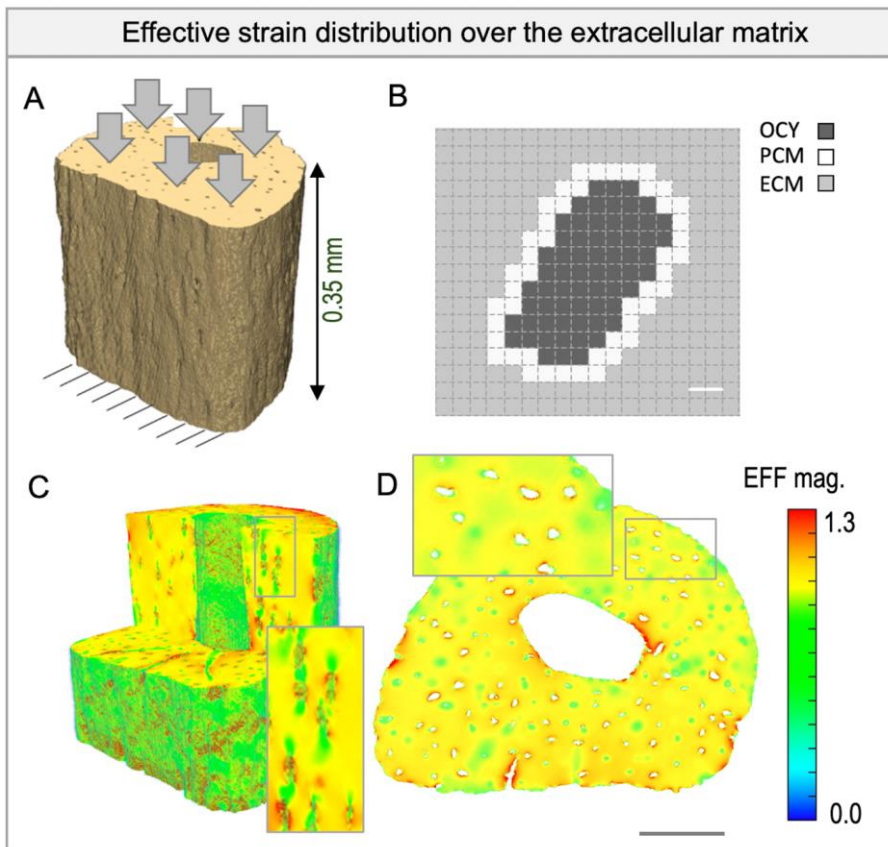


Fig 1. Representation of the micro-FE model of a midfibula diaphysis and effective strain distribution (A) Applied loading and boundary conditions; **(B)** A 2D representative osteocyte showing the extracellular matrix (ECM), the pericellular matrix (PCM) and osteocyte (OCY). Scale bar=1.4 μm . **(C)** Effective strain distribution over the entire micro-FE model of the extracellular matrix (ECM) under an apparent strain of 1%. **(D)** Contour plots of ECM effective strains (EFF) over the entire bone's cross section. Inserts magnified 2.5x. Scale bar=100 μm .

15% of osteocyte volume are exposed to a strain smaller than the applied longitudinal strain (Fig. 2); while, 85% of the OCY volume are exposed to strain levels higher than or equal to the applied strain. In nearly half (48.0%) of the OCY volume the strain magnification was higher than 1.5; 7.1% of the osteocyte volume experienced a strain magnification higher than 2.5.

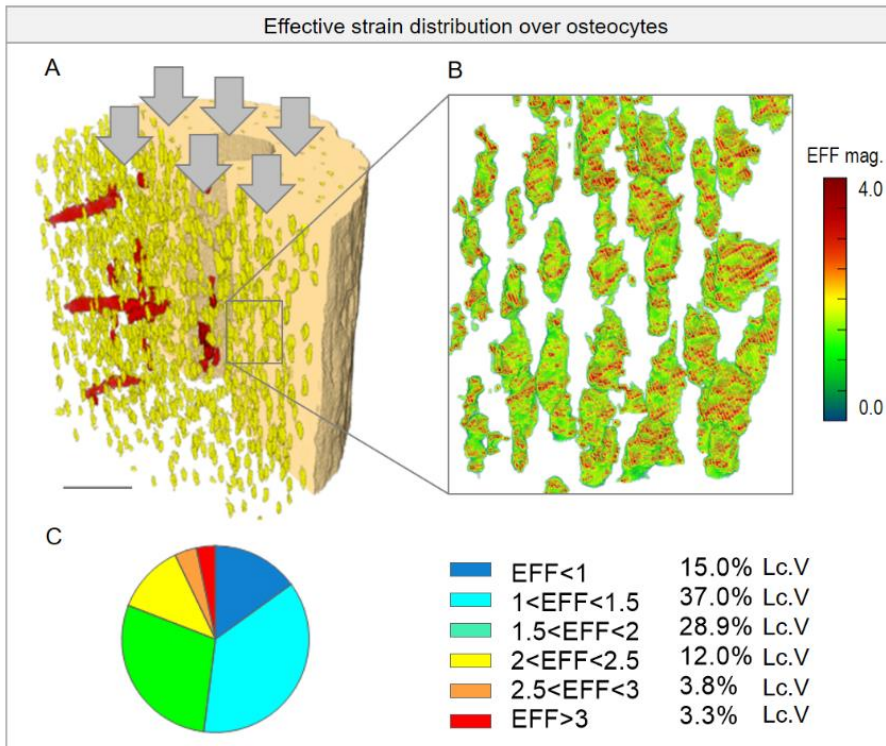


Fig 2. Effective strain distribution over osteocytes. (A) 3D rendering of mouse fibula microporosity comprising vascular canal network (red) and osteocyte lacunae (yellow). (B) Contour plots of osteocyte (OCY) effective strains (EFF). The red color shows where the strain magnification is higher than 2.5. (C) Percentage of osteocyte volume are exposed to a specific effective strain. Insert magnified 8×. Scale bar=100 μm.

The maximum EFF strains in ECM, PCM and OCYs increased with increasing lacuna volume and orientation, while the maximum EFF strains in ECM, PCM and OCYs significantly decreased as the sphericity of the lacuna increased (Fig. 3). Based on our data, it can be concluded that on average, 12.6%, 9.6%, and 5.3% higher

strains were predicted in OCYs, PCM and ECM of large lacunae (volume of 500-600 μm^3) than in small lacunae (volume of 100-200 μm^3), respectively (Fig 3 A). The more round lacunae were exposed to lower maximum EFF strains in comparison with flat ones. An approximate 25%, 23% and 13% decrease in maximum strains were found for an increase in the lacuna sphericity from 0-0.5 to 0.7-1 in OCYs, PCM and ECM, respectively (Fig 3 B). Lacunae with a long axis that deviated by more than 8 degrees from the longitudinal axis (cut-off value for orientation was selected as the median value) had significantly higher maximum EFF strains compared to lacunae with an orientation less than 8 degree. On average, the lacunae with larger deviation in orientation from the bone longitudinal axis were exposed to 8% higher maximum effective strains in OCYs, 6.5% in PCM and 4.2% in ECM, than lacunae with a deviation in orientation below 8 degrees (Fig. 3 C).

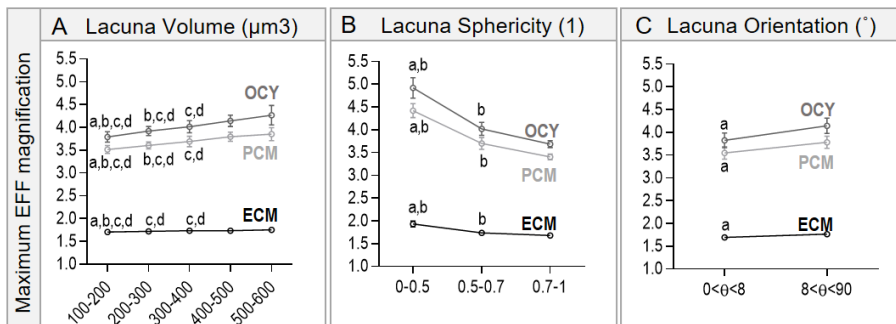


Fig 3. Effect of lacuna shape parameters on effective strains. (A) Maximum effective strains (EFF) in the extra cellular matrix (ECM), the pericellular matrix (PCM) and the osteocyte cell bodies (OCY) increase as lacuna volume increases. Values are mean \pm SD. Significant difference ($p < 0.05$) in maximum EFF between each specific group and “a” the 200-300 μm^3 (group); “b” the 300-400 μm^3 (group); “c” the 400-500 μm^3 (group); “d” the 500-600 μm^3 (group). **(B)** Maximum effective strains in ECM, PCM

and OCYs decrease as lacuna sphericity increases. Significant difference in maximum EFF between each specific group and “a” 0.6-0.75 (group); “b” 0.75-1.00 (group). **(C)** Maximum effective strains in ECM, PCM and OCYs increase as lacuna orientation increases. Significant difference in maximum EFF between $0 < \Theta < 8$ (group) and “a” $8 < \Theta < 90$ (group).

The maximum and minimum EFF strains predicted in ECM were dependent on the distance from the lacuna boundary (Fig. 4 A, B). The maximum EFF strains decreased with increasing distance from the lacuna boundary whereas the minimum EFF strains increased by increasing distance from lacuna boundary. Since, the highest maximum and the lowest minimum strains were observed within the 0.7 μm vicinity of the lacunae, the maximum and minimum EFF strain amplifications as a function of lacunae shape factors were quantified within 0.7 μm from each lacuna boundary. The maximum EFF strains dropped sharply by 28.3% from 0.7 to 1.4 μm vicinity of lacunae (Fig. 4). Moreover, the mesh refinement study showed a good agreement between the original and the finer models confirming that the original modeling approach and its outcomes are independent of the voxel size. Indeed, the profile of the effective strain as a function of the distance from the lacuna boundary was nearly identical for the 0.7 μm and 0.35 μm voxel meshes (Fig 4 C).

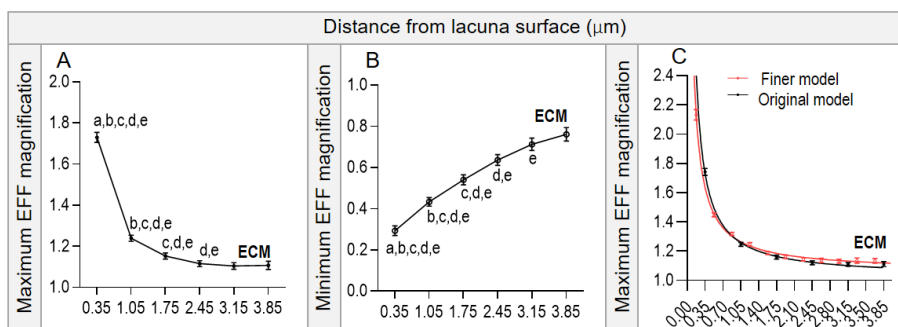


Fig 4. Effective strain magnification as a function of the distance from the lacuna boundary. (A) Maximum effective strain (EFF) in the extracellular matrix (ECM) decreases with increasing distance from the lacuna boundary. (B) Minimum effective strain in ECM increases with increasing distance from the lacuna boundary. (C) Results of mesh refinement study. The profile of the effective strain as a function of the distance from the lacuna boundary was nearly identical for the original model with 0.7 μm and finer model with 0.35 μm voxel meshes. Values are mean \pm SD; Significant difference ($p < 0.05$) in EFF between each specific group and “a” 1.4 μm ; “b” 2.1 μm ; “c” 2.8 μm ; “d” 3.5 μm ; “e” 4.2 μm .

The variations in the three-dimensional morphology of bone microporosity have been reported recently in another paper (Hemmatian et al., 2018b). Briefly, intracortical microporosity, consisting of lacunar and vascular porosities was significantly lower in 23-month-old female mice than in 5-month-old female mice ($p < 0.01$; Table 1). The number of lacunae was not affected by aging whereas the mean lacuna volume in old mice ($243.4 \pm 26.26 \mu\text{m}^3$) was significantly lower compared to young mice ($279.2 \pm 28.78 \mu\text{m}^3$) ($p < 0.05$; Table 1). The lacunae were oriented in the longitudinally direction with an average orientation of $9.96 \pm 2.12^\circ$ in young mice and $11.42 \pm 0.70^\circ$ in old mice. Significantly more rounded lacunae with a sphericity higher than 0.65 were found in old mice compared to young ones ($p < 0.05$). Multiple regression analysis revealed that lacuna volume, sphericity and orientation were all significantly correlated to maximum and minimum effective strains in ECM. The regression equations are:
Maximum EFF = $1.91e-02 + 2.03e-06 \text{ Lc.V} - 3.97e-03 \text{ Lc.Sph} + 3.30e-05 \text{ Lc.}\Theta$ ($p < 0.0001$, $R^2 = 8.53 \%$)

Minimum EFF = $2.43e-03 - 1.71e-06 \text{ Lc.V} + 1.56e-03 \text{ Lc.Sph} - 4.41e-06 \text{ Lc.}\Theta$ ($p < 0.0001$, $R^2 = 12.51 \%$)

The μ FE models showed that due to the presence of smaller and more round lacunae in old mice, local bone tissue strains were slightly, but significantly reduced (Fig 5). Specifically, the mean maximum EFF strain magnification in OCYs in the old group (3.87 ± 0.07) was 5.2% lower than in the young group (4.08 ± 0.12 ; Fig. 5 A). Furthermore, in PCM this reduction was 5.0% (Old: 3.57 ± 0.05 ; Young: 3.76 ± 0.09 ; Fig. 5 A), whereas in ECM, within a $0.7 \mu\text{m}$ vicinity of the lacunar surface this reduction was 2.3% (Old: 1.71 ± 0.01 ; Young: 1.75 ± 0.02 ; Fig. 5 A). At the same time, the minimum strain amplification in old animals were closer to 1, i.e., less reduced, than in young animals. Specifically, the mean minimum EFF strain magnification in OCYs at old age (0.93 ± 0.02) was 12.3% higher than at young age (0.86 ± 0.06 ; Fig. 5B). Furthermore, in PCM the minimum strains at old age were 23.2% higher than at young age (Old: 0.47 ± 0.02 ; Young: 0.38 ± 0.03 ; Fig. 5B), whereas in ECM within a $0.7 \mu\text{m}$ vicinity of lacunar surface the strains were 12.3% higher (Old: 0.31 ± 0.08 ; Young: 0.28 ± 0.02 ; Fig. 5B). The maximum effective strains in OCY were up to 2.3 times the maximum effective strains in the ECM; maximum effective strains in the PCM were up to 2.1 times higher than those in the ECM. The minimum effective strains were lowest in the ECM; the minimum effective strains in the ECM were 0.3 times lower than in PCM and 0.7 times smaller than in OCYs (Fig. 5). Additionally, the regional analysis showed that in both age groups, the mean maximum EFF strain magnification in OCY, PCM and ECM were independent of anatomical location (Table 2). As age increased, maximum EFF strain magnification in OCY, PCM and ECM in both anterior and posterior sites were significantly reduced (Table 2).

Deleted:

Deleted:

Deleted:

Deleted:

Deleted:

Deleted:

Deleted:

Deleted:

Deleted:

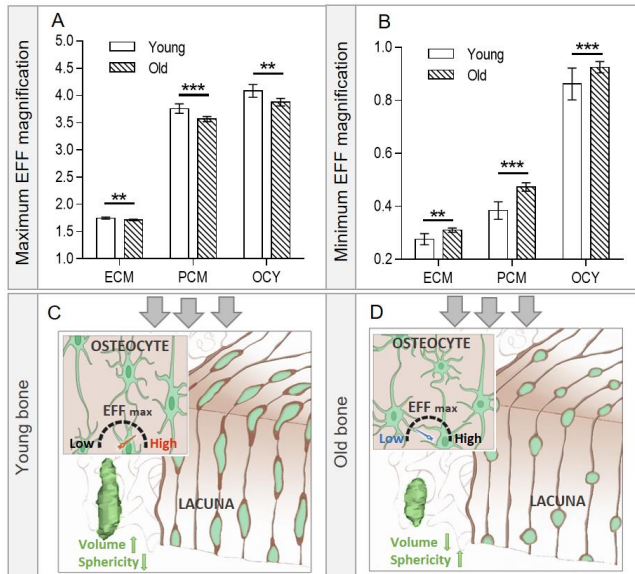


Fig 5. The effect of aging on maximum and minimum effective strains in the extracellular matrix (ECM) located within a 0.7 μm vicinity of the lacunar surface, in the pericellular matrix (PCM) and in the osteocyte cell bodies (OCYs) due to an apparent strain of 1%. (A) The maximum effective strain magnifications in OCYs were significantly higher than those in ECM and PCM. Mean maximum effective strain magnifications in ECM, PCM and OCY were significantly lower in old animals. **(B)** Mean minimum effective strains were significantly lower in young animals. The minimum effective strains were lowest in the ECM; the minimum effective strains in the ECM were 0.3 times lower than in PCM and 0.7 times smaller than in OCYs. **(C,D)** Proposed relationship between age-related changes in lacunae shape and local bone tissue strains in osteocytes. With aging the shape of the osteocyte lacunae changes from elongated towards round (increased sphericity); in addition, the lacunae reduce in size. A direct mechanical consequence would be that local strain magnification in the bone tissue around the lacunae will reduce in magnitude, assuming that overall

daily strains remain the same. Hence, osteocytes located in smaller and more round lacunae in aged bones might be exposed to lower local tissue strains than those in larger and thinner lacunae in young bones. Values are mean±SD. + Indicates significant difference between young and old mice. ++ p<0.01 and +++, *** p<0.001, **** p<0.0001.

Table 1. Morphometric parameters (Hemmatian et al., 2018b)

Parameters	Young mice	Old mice	p(t-test)
Ct.BV/TV (%)	90.42 ± 2.87	79.73 ± 12.15	0.06
Total microporosity (%)	1.49 ± 0.14	1.22 ± 0.18	0.01
Ca.V/Ct.TV (%)	0.24 ± 0.08	0.09 ± 0.06	<0.01
Lc.V/Ct.TV (%)	1.25 ± 0.13	1.13 ± 0.19	0.22
N.Lc/Ct.TV (mm ⁻³)	44835 ± 1665	46075 ± 3526	0.45
Lc.V (µm ³)	279.2 ± 28.78	243.4 ± 26.26	0.04
Lc.Sph>0.65 (%)	28.97 ± 10.99	43.55 ± 10.09	0.04
Lc.θ (°)	9.96 ± 2.12	11.42 ± 0.70	0.14

TV = total tissue volume; Ct.TV = cortical total volume (comprising the cortical bone volume together with lacunae and vascular canal network); Ct.BV = cortical bone volume; Ct.BV/TV = cortical bone volume fraction; Total microporosity = (Ca.V+Lc.V)/Ct.TV; Ca.V/Ct.TV = canal porosity; Lc.V/Ct.TV = lacuna porosity; N.Lc/Ct.TV = lacuna number density; Lc.V = mean lacuna volume; Lc.Sph = mean lacuna sphericity; Lc.θ = mean lacuna orientation. Values are mean ± SD; P<0.05.

Table 2. Maximum effective magnification at different anatomical sites.

Maximum EFF magnification	Young		Old	
	Posterior	Anterior	Posterior	Anterior
OCY	4.122 ± 0.118 ^a	4.035 ± 0.148 ^a	3.847 ± 0.046 ^a	3.888 ± 0.094 ^a
PCM	3.793 ± 0.087 ^a	3.722 ± 0.110 ^a	3.545 ± 0.023 ^a	3.577 ± 0.069 ^a
ECM	1.811 ± 0.022 ^a	1.788 ± 0.045 ^a	1.728 ± 0.020 ^a	1.729 ± 0.029 ^a

EFF = effective strain; OCY = the osteocyte cell bodies; PCM = the pericellular matrix; ECM = the extra cellular matrix; Values are mean \pm SD. a Significant differences ($p < 0.05$) between the indices at young and old age. No significant differences were found between the posterior and anterior sites.

4. DISCUSSION

In this study, we developed 3D μ FE models of the entire mouse cortical bone microstructure including more than 1500 lacunae and vascular channels to study the effects of lacunar shape and distribution on the mechanical environment of osteocytes and the surrounding matrix. Our results showed that the mechanical environment of osteocytes differs due to the morphology of lacunae. We further showed that age-related changes in lacunar morphology result in slightly lower local bone tissue strains in the vicinity of lacunae and the osteocytes inside, under identical external mechanical loads.

We found that the lacunar morphology significantly affected the mechanical environment around osteocytes and their surrounding matrix. The lacunae with a volume of 500-600 μm^3 resulted in 12.6% higher peak effective strains in osteocytes cell bodies than the lacunae with a smaller volume of 100-200 μm^3 . The maximum effective strains on osteocytes cells decreased by 25% as the sphericity of the lacunae increased from 0-0.5 to 0.7-1. The orientation of the lacunae also affected the local mechanical strain of the bone. Namely, the osteocytes residing in lacunae with larger orientation ($>8^\circ$) from the longitudinal axis of the bone are exposed to 8% higher peak effective strains than the osteocytes with lacunae orientation below 8 degrees. Our findings may also explain the preferential orientation of the osteocyte long axes in parallel to loading direction (Aviral Vatsa et al., 2008), minimizing the effects of stress concentrating and crack initiation (Currey, 2003; CURREY, 1962; Nicoletta et al., 2006). Our data are in agreement with the results found recently by Kola et al. (Kola et al., 2020) who demonstrated lower lacunar strains for the osteocytes aligned along the loading axis compared to osteocytes aligned perpendicular to loading axis and higher strains for osteocytes with larger lacunae volume. Furthermore, the maximum

EFF strains in ECM significantly decreased with increasing distance from the lacuna boundary whereas the minimum EFF strains significantly increased with increasing distance from the lacuna boundary in both young and old fibulae. This finding corroborates earlier results based on realistic geometries that the ECM strains decrease with increasing distance from the lacuna boundary (Schneider et al., 2012; Varga et al., 2015). Hence, present results support the idea that lacuna shape variations result in a nonuniform local bone tissue strain distribution.

The predicted strain levels close to the lacunae were consistent with the local cortical bone strains reported in previous numerical and experimental works (Bonivitch et al., 2007; Deligianni and Apostolopoulos, 2008; Nicoletta et al., 2006; Wang et al., 2015). We found a mean maximum strain amplification factor of 1.7 in the ECM, 3.7 in PCM and 4.1 in OCYs. Even higher strain amplification factors (up to 70) have been reported previously using confocal image-based (Verbruggen et al., 2012) and synchrotron X-ray phase nano-tomography-based FE models of lacuna canalicular network (Varga et al., 2015). However, the larger strains have been reported at the junction of canaliculi and lacunae, which have not been considered in the current study; a higher resolution is required to visualize the canalicular network. We further found that a relatively small portion (7.1%) of osteocyte volume is exposed to localized mechanical stimuli with a strain magnification higher than 2.5. As previously reported, 1-10% *in vitro* strains, working directly on the osteocytes, are required to activate osteocytes (You et al., 2000). Even at 0.3% *in vivo* bulk bone strains, as elicited by vigorous activities (Burr et al., 1996), our μ FE modeling estimates that a maximum of 1% strain only reached in a small portion (3.3%) of osteocytes. This would indicate that the overall lacuna morphological characteristics may not be solely sufficient to

magnify the mechanical stimuli high enough to have an impact on osteocyte stimulation.

The primary shape of osteocyte lacunae is defined when the former osteoblasts are buried and the surrounding matrix mineralizes (Franz-Odenaal et al., 2006) supported by the link between lacunar orientation and collagen fiber orientation in human osteonal bone demonstrated by (Marotti, 1979). It has been shown that at a later stage osteocytes also actively shape their lacuna by resorbing and building bone within their perilacunar bone matrix (Yee et al., 2019) through the processes of osteocytic osteolysis (Bélanger, 1969; Qing et al., 2012; Tazawa et al., 2004) and perilacunar bone formation (Baylink and Wergedal, 1971), respectively. The shape of the osteocytes and of their lacunae vary significantly depending on the age of the bone tissue (Carter et al., 2013; Hemmatian et al., 2018b; Milovanovic et al., 2013; Tiede-Lewis and Dallas, 2019) and the anatomical location (Aviral Vatsa et al., 2008); they may also change due to variations in hormone levels (Qing et al., 2012; Tazawa et al., 2004), as well as with bone pathologies (van Hove et al., 2009). The variations in the lacunae morphology are likely to cause changes in osteocyte shape, as nano-computed tomography and confocal laser scanning microscopy have shown similar alignment and shape of osteocytes and their lacunae (van Hove et al., 2009; Aviral Vatsa et al., 2008). In turn, changes to the morphology of osteocytes will affect the cytoskeletal structure of the osteocyte (Ajubi et al., 1996; McGarry et al., 2005; Wang et al., 1993), which has a pivotal role in the mechanoresponse of the osteocyte (Klein-Nulend et al., 2012). The outcomes of the current study may partly explain our previous findings of the greater mechanoresponse of osteocytes in fibulae of lactating mice, which are embedded in larger lacunae likely experiencing higher local strain in comparison with the osteocytes from virgin mice residing in smaller lacunae with lower

strain (Hemmatian et al., 2018a). All taken together, it can be hypothesized that the variations in the osteocyte lacunar morphology may cause changes in the local mechanical environment of the osteocyte and at least in part affecting the subsequent osteocyte mechanoresponse. Yet, it remains unknown if the alterations in local strain magnitudes around osteocytes caused by lacunar shape variations are sufficient to perceive by the cells, leading to changes in bone mechanoresponse. **It also remains unknown to what extent our findings for the fibula can be extrapolated to other bones because specific details on osteocyte volume, shape, and density for other bones are limited or non-existent.**

Since osteocytes sense matrix strains directly via their cell bodies, these local lacunar size and shape variations in old animals might result in a reduced response of osteocytes. As a result, the lower mechanoresponse in old animals would lead to bone loss whereas an identical external load in young animals could lead to higher local maximum effective strains in the bone matrix and an increased response of the osteocytes. Additionally, round osteocytes are more mechanosensitive and require less mechanical force than flat ones in order to release nitric oxide (Bacabac et al., 2008), hence, the measured alteration in lacunar shape could be one of the factors involved in age-related alterations in bone mass and architecture. On the other hand, old bones are expected to experience higher strains due to bone loss and subsequent shape modifications than young bones under identical loading conditions. However, we showed that age-related changes in lacunar shape result in slightly lower local bone tissue strains. This may provide a mechanism through which the osteocytes in old bones supposed to expose to higher strains could potentially finetune their local strain environment by adapting their lacunar shape through perilacunar remodeling at old age in order to remain within an optimal range to elicit a biological response.

One limitation of our study is that scanning at a spatial resolution of 0.7 micrometers is not enough to visualize the canalicular network. The canalicular network acts as a potential stress concentrator. The insertion sites of cell extensions with osteocyte cell bodies, where focal adhesions sites seem to be localized *in vivo* (A Vatsa et al., 2008), have been shown to be the most sensitive parts of osteocyte cell bodies (Adachi et al., 2009; Burra et al., 2010). Considering the extent of the canalicular network, studying the effect of morphological changes of this network on the mechanical environment of osteocytes may help to unravel whether any alterations are related to an altered capability of osteocytes to respond to the mechanical loading (Milovanovic et al., 2013). Keep in mind though, that this was not the goal of the current study, where we aimed to unravel the potential effect of osteocyte lacuna shape on local strain amplifications.

Another limitation is that the material properties were assumed to be homogeneous, linear, and isotropic. This simplification allowed to address the role of the osteocyte's size, shape and orientation without potential confounding effects of variations in local bone tissue properties. Though it has been shown that these assumptions are justified in quantitative analyses of bone mechanical response at the tissue level (van Rietbergen and Ito, 2015) they may represent an oversimplification of the mechanical response at the cellular level; e.g. bone tissue composition and lamellar orientation will affect bone mechanical response at the ultrastructural level (Vaughan et al., 2013, 2012). Furthermore, micropetrosis and mineralization of perilacunar space with aging (Milovanovic et al., 2017) might affect perilacunar quality and mechanical environment of osteocytes. To what extent these inhomogeneities affect local strain amplification is unknown, and experimental data to address this issue is unavailable. Furthermore, since no experimental data are available for the

material properties of the PCM, in the previous FE studies (Sugawara et al., 2008; Varga et al., 2015; Verbruggen et al., 2012), the properties of chondrocyte PCM (Alexopoulos et al., 2005, 2003) were considered as the material properties of the PCM with an elastic modulus of 40 kPa and Poisson's ratio of 0.4. However, in our study, due to limitation of the microFE solver ParOSol that all materials have to have the same Poisson's ratio, a Poisson's ratio of 0.3 has been considered for all 3 materials in FE models.

The murine model used in this study can be regarded as a relevant and appropriate model of age-related changes in humans as the decreased volume and increased sphericity in the murine osteocyte lacunae resemble the changes that are occurring with increasing age to osteocyte lacunae in human femora (Carter et al., 2013). The advantage of using murine fibulae for the analysis is that their small size facilitated analysis by μ CT since a single field of view encompassed the entire bone's cross section; hence no cutting nor preparation was required, possibly resulting in artefacts. Furthermore, the fibula is a load-bearing bone that adapts to mechanical loading; indeed, several groups have successfully used murine fibulae to study skeletal mechanobiology and demonstrated bone adaptation to mechanical loading in a similar way as in the tibia (Lambert, 1971; Moustafa et al., 2009; Sinnesael et al., 2015; Aviral Vatsa et al., 2008).

In summary, μ FE analysis of entire mouse cortical bone microstructure including over 1500 lacunae and vascular canals showed that variations in the morphology of lacunae resulted in alterations in local strain amplification. The presence of smaller and more round lacunae in old mice caused slightly lower strains in osteocytes and their surrounding matrix. Understanding how changes in lacunar morphology affect the micromechanical environment of osteocytes presents a first

step in unraveling their potential role in the amount of strains that the osteocyte cell bodies are exposed to. Although, how - and to what extent - these local strain changes are perceived by osteocytes is still a question. Further studies could address the bone mechano-biological response to nonuniform local bone tissue strain distribution to reveal whether even the most extreme shape changes of osteocyte lacunae have a large enough impact on the strains experienced by the osteocytes to make a biological consequence, e.g. impaired bone mechanoreponse seen with aging.

DISCLOSURES

Authors declare that they have no conflict of interests.

Data will be made available upon reasonable request.

ACKNOWLEDGEMENT

This research was supported by the European Commission through MOVE-AGE, an Erasmus Mundus Joint Doctorate programme (2011-0015) and by the Swiss National Supercomputing Centre (CSCS) under project ID 841. HH is supported by a postdoctoral fellowship grant from the Alexander von Humboldt foundation.

Authors' roles: Study design: HH, ADB, JKN, GHL; Data collection and analysis: HH; Data interpretation: HH, ADB, JKN, GHL; Drafting manuscript: HH, ADB, GHL; Revising manuscript content: HH, ADB, JKN, GHL; Approving final version of manuscript: HH, ADB, JKN, GHL; HH and GHL take responsibility for the integrity of the data analysis.

REFERENCES

- Adachi, T., Aonuma, Y., Tanaka, M., Hojo, M., Takano-Yamamoto, T., Kamioka, H., 2009. Calcium response in single osteocytes to locally applied mechanical stimulus: differences in cell process and cell body. *J. Biomech.* 42, 1989–1995. <https://doi.org/10.1016/j.jbiomech.2009.04.034>
- Ajubi, N.E., Klein-Nulend, J., Nijweide, P.J., Vrijheid-Lammers, T., Alblas, M.J., Burger, E.H., 1996. Pulsating fluid flow increases prostaglandin production by cultured chicken osteocytes--a cytoskeleton-dependent process. *Biochem. Biophys. Res. Commun.* 225, 62–68. <https://doi.org/10.1006/bbrc.1996.1131>
- Alexopoulos, L.G., Haider, M.A., Vail, T.P., Guilak, F., 2003. Alterations in the mechanical properties of the human chondrocyte pericellular matrix with osteoarthritis. *J. Biomech. Eng.* 125, 323–333. <https://doi.org/10.1115/1.1579047>
- Alexopoulos, L.G., Setton, L.A., Guilak, F., 2005. The biomechanical role of the chondrocyte pericellular matrix in articular cartilage. *Acta Biomater.* 1, 317–325. <https://doi.org/10.1016/j.actbio.2005.02.001>
- Anderson, E.J., Knothe Tate, M.L., 2008. Idealization of pericellular fluid space geometry and dimension results in a profound underprediction of nano-microscale stresses imparted by fluid drag on osteocytes. *J. Biomech.* 41, 1736–1746. <https://doi.org/https://doi.org/10.1016/j.jbiomech.2008.02.035>
- Bacabac, R.G., Mizuno, D., Schmidt, C.F., MacKintosh, F.C., Van Loon, J.J.W.A., Klein-Nulend, J., Smit, T.H., 2008. Round versus flat: bone cell morphology, elasticity, and mechanosensing. *J. Biomech.* 41, 1590–1598. <https://doi.org/10.1016/j.jbiomech.2008.01.031>
- Baylink, D.J., Wergedal, J.E., 1971. Bone formation by osteocytes. *Am. J. Physiol.* 221, 669–678.
- Bélanger, L.F., 1969. Osteocytic osteolysis. *Calcif. Tissue Res.* 4, 1–12. <https://doi.org/10.1007/BF02279101>
- Bonivitch, A.R., Bonewald, L.F., Nicoletta, D.P., 2007. Tissue strain amplification at the osteocyte lacuna: a microstructural finite element analysis. *J. Biomech.* 40, 2199–2206. <https://doi.org/10.1016/j.jbiomech.2006.10.040>
- Burger, E.H., Klein-Nulend, J., 1999. Mechanotransduction in bone--role of the lacuno-canalicular network. *FASEB J. Off. Publ. Fed. Am. Soc. Exp. Biol.* 13 Suppl, S101-12.
- Burr, D.B., Milgrom, C., Fyhrie, D., Forwood, M., Nyska, M., Finestone, A., Hoshaw, S., Saiag, E., Simkin, A., 1996. In vivo measurement of human tibial strains during vigorous activity. *Bone* 18, 405–410. [https://doi.org/10.1016/8756-3282\(96\)00028-2](https://doi.org/10.1016/8756-3282(96)00028-2)
- Burra, S., Nicoletta, D.P., Francis, W.L., Freitas, C.J., Mueschke, N.J., Poole, K., Jiang, J.X., 2010. Dendritic processes of osteocytes are mechanotransducers that induce the opening of hemichannels. *Proc. Natl. Acad. Sci. U. S. A.* 107, 13648–13653. <https://doi.org/10.1073/pnas.1009382107>

- Carter, Y., Thomas, C.D.L., Clement, J.G., Cooper, D.M.L., 2013. Femoral osteocyte lacunar density, volume and morphology in women across the lifespan. *J. Struct. Biol.* 183, 519–526. <https://doi.org/10.1016/j.jsb.2013.07.004>
- Chen, C.S., Tan, J., Tien, J., 2004. Mechanotransduction at cell-matrix and cell-cell contacts. *Annu. Rev. Biomed. Eng.* 6, 275–302. <https://doi.org/10.1146/annurev.bioeng.6.040803.140040>
- Currey, J.D., 2003. The many adaptations of bone. *J. Biomech.* 36, 1487–1495. [https://doi.org/10.1016/s0021-9290\(03\)00124-6](https://doi.org/10.1016/s0021-9290(03)00124-6)
- CURREY, J.D., 1962. Stress Concentrations in Bone. *J. Cell Sci.* s3-103, 111–133.
- Deligianni, D.D., Apostolopoulos, C.A., 2008. Multilevel finite element modeling for the prediction of local cellular deformation in bone. *Biomech. Model. Mechanobiol.* 7, 151–159. <https://doi.org/10.1007/s10237-007-0082-1>
- Flaig, C., Arbenz, P., 2011. A scalable memory efficient multigrid solver for micro-finite element analyses based on CT images. *Parallel Comput.* 37, 846–854. <https://doi.org/10.1016/j.parco.2011.08.001>
- Franz-Odenaal, T.A., Hall, B.K., Witten, P.E., 2006. Buried alive: how osteoblasts become osteocytes. *Dev. Dyn. an Off. Publ. Am. Assoc. Anat.* 235, 176–190. <https://doi.org/10.1002/dvdy.20603>
- FROST, H.M., 1960. Micropetrosis. *J. Bone Joint Surg. Am.* 42-A, 144–150.
- Hemmatian, H., Jalali, R., Semeins, C.M., Hogervorst, J.M.A., van Lenthe, G.H., Klein-Nulend, J., Bakker, A.D., 2018a. Mechanical Loading Differentially Affects Osteocytes in Fibulae from Lactating Mice Compared to Osteocytes in Virgin Mice: Possible Role for Lacuna Size. *Calcif. Tissue Int.* 103, 675–685. <https://doi.org/10.1007/s00223-018-0463-8>
- Hemmatian, H., Laurent, M.R., Bakker, A.D., Vanderschueren, D., Klein-Nulend, J., van Lenthe, G.H., 2018b. Age-related changes in female mouse cortical bone microporosity. *Bone* 113, 1–8. <https://doi.org/10.1016/j.bone.2018.05.003>
- Hemmatian, H., Laurent, M.R., Ghazanfari, S., Vanderschueren, D., Bakker, A.D., Klein-Nulend, J., van Lenthe, G.H., 2017. Accuracy and reproducibility of mouse cortical bone microporosity as quantified by desktop microcomputed tomography. *PLoS One* 12, e0182996. <https://doi.org/10.1371/journal.pone.0182996>
- Klein-Nulend, J., Bacabac, R.G., Bakker, A.D., 2012. Mechanical loading and how it affects bone cells: the role of the osteocyte cytoskeleton in maintaining our skeleton. *Eur. Cell. Mater.* 24, 278–291.
- Klein-Nulend, J., Bakker, A.D., Bacabac, R.G., Vatsa, A., Weinbaum, S., 2013. Mechanosensation and transduction in osteocytes. *Bone* 54, 182–190. <https://doi.org/10.1016/j.bone.2012.10.013>
- Kola, S.K., Begonia, M.T., Tiede-Lewis, L.M., Laughrey, L.E., Dallas, S.L., Johnson, M.L., Ganesh, T., 2020. Osteocyte lacunar strain determination using multiscale finite element analysis. *Bone Reports* 12, 100277. <https://doi.org/https://doi.org/10.1016/j.bonr.2020.100277>

- Lambert, K., 1971. The weight-bearing function of the fibula: a strain gauge study. *J Bone Jt. Surg* 53, 507–13.
- Marotti, G., 1979. Osteocyte orientation in human lamellar bone and its relevance to the morphometry of periosteocytic lacunae. *Metab. Bone Dis. Relat. Res.* 1, 325–333. [https://doi.org/http://dx.doi.org/10.1016/0221-8747\(79\)90027-4](https://doi.org/http://dx.doi.org/10.1016/0221-8747(79)90027-4)
- McCreadie, B.R., Hollister, S.J., Schaffler, M.B., Goldstein, S. a., 2004. Osteocyte lacuna size and shape in women with and without osteoporotic fracture. *J. Biomech.* 37, 563–572. [https://doi.org/10.1016/S0021-9290\(03\)00287-2](https://doi.org/10.1016/S0021-9290(03)00287-2)
- McGarry, J.G., Klein-Nulend, J., Prendergast, P.J., 2005. The effect of cytoskeletal disruption on pulsatile fluid flow-induced nitric oxide and prostaglandin E2 release in osteocytes and osteoblasts. *Biochem. Biophys. Res. Commun.* 330, 341–348. <https://doi.org/https://doi.org/10.1016/j.bbrc.2005.02.175>
- McNamara, L.M., Majeska, R.J., Weinbaum, S., Friedrich, V., Schaffler, M.B., 2009. Attachment of osteocyte cell processes to the bone matrix. *Anat. Rec. (Hoboken)*. 292, 355–363. <https://doi.org/10.1002/ar.20869>
- Milovanovic, P., Zimmermann, E.A., Hahn, M., Djonc, D., Püschel, K., Djuric, M., Amling, M., Busse, B., 2013. Osteocytic canalicular networks: morphological implications for altered mechanosensitivity. *ACS Nano* 7, 7542–7551. <https://doi.org/10.1021/nn401360u>
- Milovanovic, P., Zimmermann, E.A., Vom Scheidt, A., Hoffmann, B., Sarau, G., Yorgan, T., Schweizer, M., Amling, M., Christiansen, S., Busse, B., 2017. The Formation of Calcified Nanospherites during Micropetrosis Represents a Unique Mineralization Mechanism in Aged Human Bone. *Small* 13. <https://doi.org/10.1002/sml.201602215>
- Moustafa, A., Sugiyama, T., Saxon, L.K., Zaman, G., Sunter, A., Armstrong, V.J., Javaheri, B., Lanyon, L.E., Price, J.S., 2009. The mouse fibula as a suitable bone for the study of functional adaptation to mechanical loading. *Bone*. <https://doi.org/10.1016/j.bone.2008.12.026>
- Nicolella, D.P., Moravits, D.E., Gale, A.M., Bonewald, L.F., Lankford, J., 2006. Osteocyte lacunae tissue strain in cortical bone. *J. Biomech.* 39, 1735–1743. <https://doi.org/10.1016/j.jbiomech.2005.04.032>
- Pistoia, W., van Rietbergen, B., Lochmuller, E.-M., Lill, C.A., Eckstein, F., Rueggsegger, P., 2002. Estimation of distal radius failure load with micro-finite element analysis models based on three-dimensional peripheral quantitative computed tomography images. *Bone* 30, 842–848.
- Qing, H., Ardeshirpour, L., Divieti Pajevic, P., Dusevich, V., Jähn, K., Kato, S., Wysolmerski, J., Bonewald, L.F., 2012. Demonstration of osteocytic perilacunar/canalicular remodeling in mice during lactation. *J. Bone Miner. Res.* 27, 1018–1029. <https://doi.org/10.1002/jbmr.1567>
- Schneider, P., Ruffoni, D., Larsson, D., Chiapparini, I., Müller, R., 2012. IMAGE-BASED FINITE ELEMENT MODELS FOR THE INVESTIGATION OF OSTEOCYTE MECHANOTRANSDUCTION. *J. Biomech.* 45, S436. [https://doi.org/https://doi.org/10.1016/S0021-9290\(12\)70437-2](https://doi.org/https://doi.org/10.1016/S0021-9290(12)70437-2)

- Sinnesael, M., Laurent, M.R., Jardi, F., Dubois, V., Deboel, L., Delisser, P., Behets, G.J., D'Haese, P.C., Carmeliet, G., Claessens, F., Vanderschueren, D., 2015. Androgens inhibit the osteogenic response to mechanical loading in adult male mice. *Endocrinology* 156, 1343–1353. <https://doi.org/10.1210/en.2014-1673>
- Sugawara, Y., Ando, R., Kamioka, H., Ishihara, Y., Murshid, S.A., Hashimoto, K., Kataoka, N., Tsujioka, K., Kajiya, F., Yamashiro, T., Takano-Yamamoto, T., 2008. The alteration of a mechanical property of bone cells during the process of changing from osteoblasts to osteocytes. *Bone* 43, 19–24. <https://doi.org/10.1016/j.bone.2008.02.020>
- Tazawa, K., Hoshi, K., Kawamoto, S., Tanaka, M., Ejiri, S., Ozawa, H., 2004. Osteocytic osteolysis observed in rats to which parathyroid hormone was continuously administered. *J. Bone Miner. Metab.* 22, 524–529. <https://doi.org/10.1007/s00774-004-0519-x>
- Tiede-Lewis, L.M., Dallas, S.L., 2019. Changes in the osteocyte lacunocanalicular network with aging. *Bone* 122, 101–113. <https://doi.org/https://doi.org/10.1016/j.bone.2019.01.025>
- Torcasio, A., Zhang, X., Duyck, J., Van Lenthe, G.H., 2012. 3D characterization of bone strains in the rat tibia loading model. *Biomech. Model. Mechanobiol.* 11, 403–410. <https://doi.org/10.1007/s10237-011-0320-4>
- van Hove, R.P., Nolte, P.A., Vatsa, A., Semeins, C.M., Salmon, P.L., Smit, T.H., Klein-Nulend, J., 2009. Osteocyte morphology in human tibiae of different bone pathologies with different bone mineral density--is there a role for mechanosensing? *Bone* 45, 321–329. <https://doi.org/10.1016/j.bone.2009.04.238>
- van Rietbergen, B., Ito, K., 2015. A survey of micro-finite element analysis for clinical assessment of bone strength: the first decade. *J. Biomech.* 48, 832–841. <https://doi.org/10.1016/j.jbiomech.2014.12.024>
- van Rietbergen, B., Weinans, H., Huiskes, R., Odgaard, A., 1995. A new method to determine trabecular bone elastic properties and loading using micromechanical finite-element models. *J. Biomech.* 28, 69–81.
- Varga, P., Hesse, B., Langer, M., Schrof, S., Männicke, N., Suhonen, H., Pacureanu, A., Pahr, D., Peyrin, F., Raum, K., 2015. Synchrotron X-ray phase nanotomography-based analysis of the lacunar-canalicular network morphology and its relation to the strains experienced by osteocytes in situ as predicted by case-specific finite element analysis. *Biomech. Model. Mechanobiol.* 14, 267–282. <https://doi.org/10.1007/s10237-014-0601-9>
- Vatsa, Aviral, Breuls, R.G., Semeins, C.M., Salmon, P.L., Smit, T.H., Klein-Nulend, J., 2008. Osteocyte morphology in fibula and calvaria --- is there a role for mechanosensing? *Bone* 43, 452–458. <https://doi.org/10.1016/j.bone.2008.01.030>
- Vatsa, A., Semeins, C.M., Smit, T.H., Klein-Nulend, J., 2008. Paxillin localisation in osteocytes—Is it determined by the direction of loading? *Biochem. Biophys. Res. Commun.* 377, 1019–1024. <https://doi.org/https://doi.org/10.1016/j.bbrc.2007.12.174>

- Vaughan, T.J., McCarthy, C.T., McNamara, L.M., 2012. A three-scale finite element investigation into the effects of tissue mineralisation and lamellar organisation in human cortical and trabecular bone. *J. Mech. Behav. Biomed. Mater.* 12, 50–62. <https://doi.org/10.1016/j.jmbbm.2012.03.003>
- Vaughan, T.J., Verbruggen, S.W., McNamara, L.M., 2013. Are all osteocytes equal? Multiscale modelling of cortical bone to characterise the mechanical stimulation of osteocytes. *Int. j. numer. method. biomed. eng.* 29, 1361–1372. <https://doi.org/10.1002/cnm.2578>
- Verbruggen, S.W., Mc Garrigle, M.J., Haugh, M.G., Voisin, M.C., McNamara, L.M., 2015. Altered mechanical environment of bone cells in an animal model of short- and long-term osteoporosis. *Biophys. J.* 108, 1587–1598. <https://doi.org/10.1016/j.bpj.2015.02.031>
- Verbruggen, S.W., Vaughan, T.J., McNamara, L.M., 2012. Strain amplification in bone mechanobiology: a computational investigation of the in vivo mechanics of osteocytes. *J. R. Soc. Interface* 9, 2735–2744. <https://doi.org/10.1098/rsif.2012.0286>
- Wang, L., Dong, J., Xian, C.J., 2015. Strain amplification analysis of an osteocyte under static and cyclic loading: a finite element study. *Biomed Res. Int.* 2015, 376474. <https://doi.org/10.1155/2015/376474>
- Wang, N., Butler, J.P., Ingber, D.E., 1993. Mechanotransduction across the cell surface and through the cytoskeleton. *Science* (80-.). 260, 1124 LP – 1127.
- Yee, C.S., Schurman, C.A., White, C.R., Alliston, T., 2019. Investigating Osteocytic Perilacunar/Canalicular Remodeling. *Curr. Osteoporos. Rep.* 17, 157–168. <https://doi.org/10.1007/s11914-019-00514-0>
- You, J., Yellowley, C.E., Donahue, H.J., Zhang, Y., Chen, Q., Jacobs, C.R., 2000. Substrate deformation levels associated with routine physical activity are less stimulatory to bone cells relative to loading-induced oscillatory fluid flow. *J. Biomech. Eng.* 122, 387–393. <https://doi.org/10.1115/1.1287161>